Many-electron hyperpolarizability density analysis: Application to the dissociation process of one-dimensional H_2

Masayoshi Nakano,[1] Hidemi Nagao,[2] and Kizashi Yamaguchi[1]
[1]*Department of Chemistry, Faculty of Science, Osaka University, Toyonaka, Osaka 560, Japan*
[2]*Osaka National Research Institute, 1-8-31 Midorioka, Ikeda, Osaka, 563, Japan*
(Received 9 July 1996; revised manuscript received 3 October 1996)

A method for density analysis of static polarizabilities (α) and second hyperpolarizabilities (γ) on the basis of the finite-field (FF) many-electron wave packets (MEWP) method is developed and applied to evaluation of the longitudinal α and γ in the dissociation process for a one-dimensional H_2 model. Remarkable increases in α and γ are observed in the intermediate dissociation region. The internuclear distance where the γ is maximized is also found to be larger than that where the α is maximized. In order to elucidate the characteristics of α and γ in the dissociation process, we extract their classical pictures describing displacements of two-electron configurations by using (hyper)polarizability densities on the two-electron coordinate plane. It is suggested from these classical pictures that the polarization in the ionic structure contributes primarily to the enhancement of (hyper)polarizability in the intermediate dissociation region, while the polarization in the diradical structure causes the decrease of the (hyper)polarizability at a large internuclear distance. This implies that the experimental search for species with chemical bonds in the intermediate correlation regime is important and interesting in relation to the molecular design of nonlinear optical materials. [S1050-2947(97)09102-6]

PACS number(s): 42.65.An, 42.50.−p, 33.20.−t, 33.15.−e

I. INTRODUCTION

Recently, the variation in polarizability in the dissociation process of H_2 has been studied to elucidate relationships between a linear optical process and electron correlations, and it has been found that the polarizability has a maximum in the intermediate dissociation region [1,2]. This feature was discussed in relation to the Hartree-Fock (HF) instabilities of chemical bonds by Champagne *et al.* [2]. However, the nonlinear optical response for molecules in the intermediate and strong correlation regime is now one of the current topics in chemical physics. In previous papers [3,4], we proposed the viewpoint that the (hyper)polarizability is a measure of the ability of electron fluctuation (electron fluctuatability) and developed a method for analysis of (hyper)polarizability based on a concept of the (hyper)polarizability density. This quantity is found to sensitively reflect the nature of electron correlations [3,4]. In order to elucidate relationships between a nonlinear optical process and electron correlations, the variations in (hyper)polarizability densities for second hyperpolarizability (γ) of H_2 in the dissociation process are investigated compared with those in polarizability (α).

H_2 is a primary test case for any quantum-chemical calculation of energies and properties. We consider one-dimensional H_2 that is one of the simplest models for reproducing the characteristics of the longitudinal (hyper)polarizability for real three-dimensional H_2. The methods including sufficient electron correlations and using extended basis sets are essential for obtaining the correct variations in energies and properties in the dissociation process. In a previous paper [5], we proposed a calculation method using electron wave packets, providing numerically exact solutions to the nonrelativistic Schrödinger equation with the *ab initio* many-electron Hamiltonian under the Born-Oppenheimer approximation. This method, denoted here as the many-electron wave packets (MEWP) method, is characterized by a direct treatment of numerically exact many-electron wave functions with arbitrary spin states on a multidimensional real coordinate and spin spaces, in contrast to the case of standard molecular orbital (MO) based methods. Although the standard methods can compute energies and properties for the ground and low-lying excited states more accurately than the present MEWP method, the MEWP method is expected to be useful for studies on behaviors of electrons near the Wannier ridge and under strong external fields. The MEWP method can be also easily extended to a time-dependent scheme that can treat transient behaviors, e.g., responses under pulsed laser, which cannot be treated by the standard time-dependent schemes, e.g., the time-dependent Hartree-Fock (TDHF) method. Further, the MEWP method is helpful in obtaining pictorial and intuitive physical pictures for various quantum phenomena since this method can directly provide graphical images of wave functions in real coordinate and spin spaces. A purpose of this study is to propose pictorial methods for analysis of (hyper) polarizabilities. Therefore, the finite-field MEWP (FF-MEWP) method is employed to calculate total energies and charge densities for the singlet ground state of one-dimensional H_2 in the presence of static electric fields. The (hyper)polarizabilities and their densities are obtained by using the numerical differentiation of the total energies and charge densities with respect to the applied fields. In addition to the (hyper)polarizability density analysis based on the reduced one-electron density, an analysis based on many-electron density is proposed to extract classical pictures of polarization primarily contributing to the (hyper)polarizability. Using this method, the characteristics of α and γ of one-dimensional H_2 in the dissociation process are discussed in connection with classical displacements of two electrons.

This paper is organized as follows. The FF-MEWP

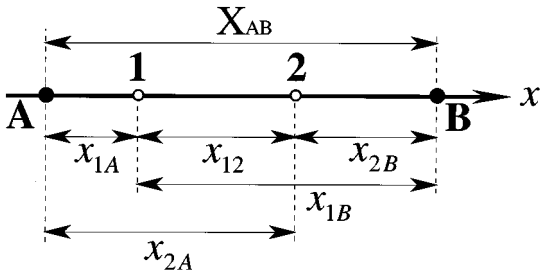

FIG. 1. One-dimensional H_2 composed of two nuclei (**A** and **B**) and two electrons (**1** and **2**).

method for one-dimensional H_2 and a numerical calculation procedure of (hyper)polarizabilities are presented in Sec. II. In Sec. III, a concept of many-electron (hyper)polarizability density is introduced as well as conventional reduced one-electron (hyper)polarizability density. Some classical pictures for a one-dimensional two-electron system are extracted by using two-electron (hyper)polarizability densities on the two-electron coordinate plane. In Sec. IV, the variations in α and γ for one-dimensional H_2 in the dissociation process are investigated by using the two-electron and reduced one-electron (hyper)polarizability density plots. The classical pictures of polarization corresponding to displacements of two-electron configurations are extracted at some internuclear distances. This is followed by a conclusion in Sec. V.

II. FINITE-FIELD MANY-ELECTRON WAVE PACKETS (FF-MEWP) METHOD

A. One-dimensional H_2 under static electric fields

We first explain a reduced version of the MEWP method that was originally developed in order to investigate quantum dynamics in real coordinate and spin spaces [5]. In a reduced version of the FF-MEWP method, the wave-packet dynamics are performed in the spatial coordinates for a two-electron system at a fixed spin state. One-dimensional H_2 is examined here, as shown in Fig. 1. In the Born-Oppenheimer approximation, the electronic Hamiltonian involving the interaction with static electric field F is written as

$$H_e=-\frac{1}{2}\frac{\partial^2}{\partial x_1^2}-\frac{1}{2}\frac{\partial^2}{\partial x_2^2}-\frac{1}{x_{1A}}-\frac{1}{x_{1B}}-\frac{1}{x_{2A}}-\frac{1}{x_{2B}}+\frac{1}{x_{12}}+Fx_1+Fx_2, \tag{1}$$

where x_1 and x_2 denote the coordinates for electrons **1** and **2**, respectively, and x_{ij} indicates the distance between particles i and j. The atomic units $\hbar=m_e=e=1$ (a.u.) are used throughout this article. The solution to a time-dependent Schrödinger equation involving the electronic Hamiltonian,

$$i\frac{\partial}{\partial t}\Phi(x_1,x_2,t)=H_e\Phi(x_1,x_2,t), \tag{2}$$

is the electronic wave function,

$$\Phi(x_1,x_2,t)=\psi(x_1,x_2,t)\varphi(\omega_1,\omega_2,t), \tag{3}$$

where $\psi(x_1,x_2,t)$ and $\varphi(\omega_1,\omega_2,t)$ represent, respectively, the spatial and spin wave functions, in which ω_1 and ω_2 indicate each spin coordinate. The singlet state of the two-electron system is considered here, since we focus on the ground-state (hyper)polarizability of H_2. For the singlet-state two-electron system, the spatial wave function, which must be symmetric with respect to the interchange of the spatial coordinates of two electrons, is generally represented as

$$\psi_s(x_1,x_2,t)=\phi_1(x_1,t)\phi_2(x_2,t)+\phi_2(x_1,t)\phi_1(x_2,t), \tag{4}$$

where $\phi_i(x,t)$ is the ith single-particle wave function. Therefore, the time-dependent Schrödinger equation to solve is

$$i\frac{\partial}{\partial t}\psi_s(x_1,x_2,t)=H_e\psi_s(x_1,x_2,t). \tag{5}$$

The singlet spatial wave function $\psi_s(x_1,x_2,t)$ is simply written as $\psi(x_1,x_2,t)$ for convenience hereafter. In the FF-MEWP method, a Gaussian wave packet is considered as the initial ith single-particle wave function expressed as

$$\phi_i(x_j,t=0)=C\ \exp\left[ip(x_j-x_{i0})-\frac{|x_j-x_{i0}|^2}{2\sigma^2}\right]. \tag{6}$$

Here, p, x_{i0}, and σ indicate momentum, coordinate of the center, and width of the ith initial wave packet, respectively. The symbol C denotes a normalization constant. Using Eqs. (4) and (6), an initial singlet wave function is constructed. This wave function is superposed by singlet eigenstates involving ground and excited states of the Hamiltonian H_e. Since our desired wave function is the ground state that is generated by the relaxation method, as shown in Eq. (11) later, the form of Eq. (6) is not so important. But it is significant that the spatial part of the ground-state singlet wavefunction for two-electron system is symmetric with respect to the exchange of two-electron coordinates as shown in Eq. (4).

In this study, we discretize the wave function in real space. Therefore, the Coulomb potential is approximated by the following softened Coulombic form [6] in order to eliminate the singularity at the origin:

$$\frac{1}{x_{ij}}\approx\frac{1}{\sqrt{a+x_{ij}^2}}, \tag{7}$$

where a is a parameter. Javanainen *et al.* gave $a=1$ for calculations of above-threshold ionization (ATI) spectra for the one-dimensional H atom [6]. This potential falls off like the Coulomb potential at large $|x_{ij}|$, but takes an asymptotic form of the Coulomb potential at short $|x_{ij}|$.

After discretizing in space, as shown in Fig. 2, the kinetic part on the right-hand side of Eq. (5) is approximated as

$$-\frac{\psi(n_2+1,n_1,t)-2\psi(n_2,n_1,t)+\psi(n_2-1,n_1,t)}{2(\Delta x)^2}$$

$$-\frac{\psi(n_2,n_1+1,t)-2\psi(n_2,n_1,t)+\psi(n_2,n_1-1,t)}{2(\Delta x)^2}. \tag{8}$$

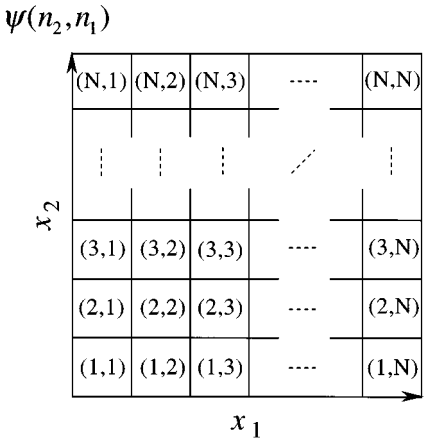

FIG. 2. Discretized coordinate plane for the one-dimensional two-electron system. A finite one-dimensional space is divided into N fragments. The numbers n_1 and n_2 represent the grid numbers of electrons **1** and **2**, respectively.

Here, $\psi(n_2,n_1,t)$ represents the wave function at the site (x_2,x_1), in which $x_i=(n_i-1)\Delta x$ $[n_i=0,1,..,N+1$ $(i=1,2)]$. Similarly the potential part using the softened Coulombic form [Eq. (7)] is written as

$$\left[-\frac{1}{\sqrt{|(n_1-n_A)\Delta x|^2+1}}-\frac{1}{\sqrt{|(n_2-n_A)\Delta x|^2+1}} -\frac{1}{\sqrt{|(n_1-n_B)\Delta x|^2+1}}-\frac{1}{\sqrt{|(n_2-n_B)\Delta x|^2+1}} +\frac{1}{\sqrt{|(n_1-n_2)\Delta x|^2+1}}+F(n_1-1)\Delta x +F(n_2-1)\Delta x \right]\psi(n_2,n_1,t), \tag{9}$$

where nuclei **A** and **B** are located at the coordinates $(n_A-1)\Delta x$ and $(n_B-1)\Delta x$, respectively. In this work, we adopt the fixed boundary condition as

$$\begin{aligned}\psi(n_2,n_1=0,t)&=\psi(n_2=0,n_1,t)\\&=\psi(n_2,n_1=N+1,t)\\&=\psi(n_2=N+1,n_1,t)=0.\end{aligned} \tag{10}$$

The time propagation of $\psi(x_1,x_2,t)$ is carried out by solving Eq. (5) in the Runge-Kutta-Tanaka scheme [7], which is an eight-step procedure with a sixth-order accuracy. According to Kosloff and Tal-Ezer [8], the singlet ground-state wave function under static electric fields can be obtained by propagating initial wavepackets in imaginary time, i.e., by setting $\tau=it$ in Eq. (5). After sufficient long-time propagation, the wave packets relax to the ground state, since all excited states involved in the initial wave packets decay to zero. The singlet ground-state wave function is represented by

$$\psi_g(x_1,x_2)=\lim_{\tau\to\infty}\frac{\psi(x_1,x_2,\tau)}{\int\int|\psi(x_1,x_2,\tau)|^2dx_1dx_2}, \tag{11}$$

where $\psi(x_1,x_2,\tau)=\psi(x_1,x_2,t)|_{it=\tau}$.

B. Calculation of (hyper)polarizability of one-dimensional H_2

The change in energy (ΔE) of a one-dimensional system under a uniform external electric field (F) is written as [3]

$$\Delta E=-\mu F-\tfrac{1}{2}\alpha FF-\tfrac{1}{3}\beta FFF-\tfrac{1}{4}\gamma FFFF-\cdots, \tag{12}$$

where the μ, α, β, and γ are dipole moment, polarizability, first, and second hyperpolarizabilities, respectively. We calculate the static α and the static γ of one-dimensional H_2 by using a numerical differentiation method. The longitudinal static α and γ are calculated by

$$\alpha=-[E(F)+E(-F)-2E(0)]/F^2, \tag{13}$$

and

$$\gamma=-[-E(3F)+12E(2F)-39E(F)+56E(0)-39E(-F)+12E(-2F)-E(-3F)]/36(F)^4, \tag{14}$$

where the total energy under static electric field, $E(F)$, is obtained as

$$E(F)=E_e(F)+\frac{1}{\sqrt{|(n_A-n_B)\Delta x|^2+1}}-F(n_A-1)\Delta x-F(n_B-1)\Delta x. \tag{15}$$

On the right-hand side of the above formula, $E_e(F)$ denotes the electronic energy under the static electric field, the second term represents the nuclear repulsion, and the remaining terms describe the interaction between nuclei and electric field.

III. (HYPER)POLARIZABILITY DENSITY ANALYSIS BY USING REDUCED ONE-ELECTRON AND MANY-ELECTRON DENSITIES

In this section, we introduce the reduced one-electron and many-electron (hyper)polarizability densities of the one-dimensional many-electron system for simplicity. These concepts can be straightforwardly extended to the case of two- and three-dimensional systems.

A. Reduced one-electron (hyper)polarizability density

The reduced one-electron density under static electric field F for the one-dimensional system is expanded as [3,9–11]

$$\rho(r,F)=\rho^{(0)}(r)+\rho^{(1)}(r)F+\frac{1}{2!}\rho^{(2)}(r)FF+\frac{1}{3!}\rho^{(3)}(r)FFF+\cdots. \tag{16}$$

The induced dipole moment is expressed as

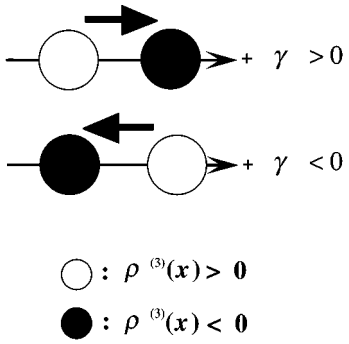

FIG. 3. Schematic diagram of the second hyperpolarizability (γ) densities [$\rho^{(3)}(x)$]. The white and black circles denote, respectively, positive and negative $\rho^{(3)}(x)$'s. The size of the circle represents the magnitude of $\rho^{(3)}(x)$ and the arrow shows the sign of $\rho^{(3)}(x)$ determined by the relative spatial configuration between these two $\rho^{(3)}(x)$'s.

$$\mu_{\mathrm{tot}}=\mu_0+\alpha F+\beta FF+\gamma FFF+\cdots , \tag{17}$$

where μ_0 denotes the ground-state permanent dipole moment. From Eqs. (16) and (17), the α and γ are represented by [3,9–11]

$$\alpha=-\int x\rho^{(1)}(x)dx \tag{18}$$

and

$$\gamma=-\frac{1}{3!}\int x\rho^{(3)}(x)dx, \tag{19}$$

where the $\rho^{(1)}(x)$ and $\rho^{(3)}(x)$, which are defined as the reduced one-electron α and γ densities, respectively, are obtained by

$$\rho^{(1)}(x)=\left.\frac{\partial\rho(x,F)}{\partial F}\right|_{F=0} \tag{20}$$

and

$$\rho^{(3)}(x)=\left.\frac{\partial^3\rho(x,F)}{\partial F^3}\right|_{F=0}. \tag{21}$$

These quantities are also simply referred to as α and γ densities, respectively. These are calculated at each spatial point in the discretized space by using the following numerical differentiation formulas:

$$\rho^{(1)}(x)=\{\rho(x,F)-\rho(x,-F)\}/2F \tag{22}$$

and

$$\rho^{(3)}(x)=\{\rho(x,2F)-\rho(x,-2F) -2[\rho(x,F)-\rho(x,-F)]\}/2(F)^3, \tag{23}$$

where $\rho(x,F)$ represents the reduced one-electron density at a spatial point x in the presence of the field F.

In order to explain a method of analysis employing the plots of reduced one-electron (hyper)polarizability densities, we consider the pair of localized $\rho^{(3)}(x)$ shown in Fig. 3

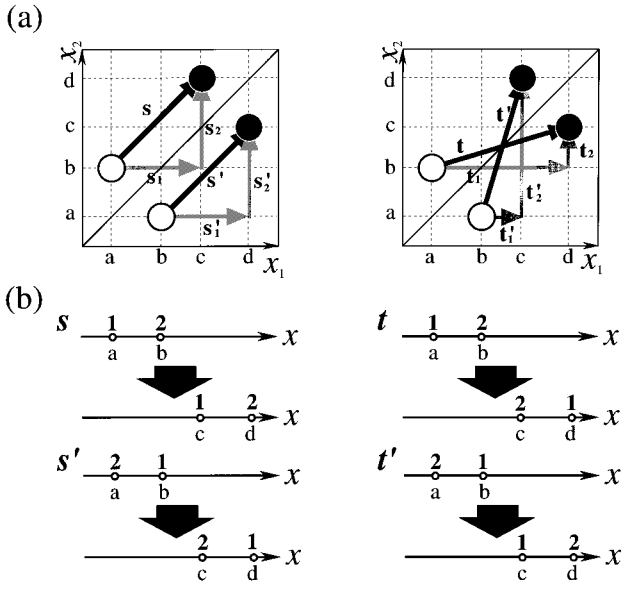

FIG. 4. (a) Two-electron (hyper)polarizability density plots corresponding to two methods of drawing vector $\mathbf{s}(\mathbf{s}')$ and $\mathbf{t}(\mathbf{t}')$ from positive to negative two-electron (hyper)polarizability densities for the one-dimensional system. The white and black circles indicate positive and negative densities, respectively. The decomposed vectors $\mathbf{s}_i(\mathbf{s}_i')$ and $\mathbf{t}_i(\mathbf{t}_i')$ $(i=1,2)$ are also shown. (b) Classical pictures of polarization extracted from vectors $\mathbf{s}$, $\mathbf{s}'$, $\mathbf{t}$, and $\mathbf{t}'$. Two electrons (**1** and **2**) are represented by white circles; and a, b, c, and d denote the positions of the one-dimensional coordinate.

[3,10,11]. The positive sign of the $\rho^{(3)}(x)$ implies that the second derivative of the charge density increases with the increase in the field. As can be seen from Eq. (19), the arrow from positive to negative $\rho^{(3)}(x)$ shows the sign of the contribution to γ determined by the relative spatial configuration between the two $\rho^{(3)}(x)$'s. Namely, the sign of the contribution to γ becomes positive when the direction of the thick arrow coincides with the positive direction of the coordinate system. The contribution to γ determined by the $\rho^{(3)}(x)$'s of the two points is more significant, when their distance is larger.

B. Many-electron (hyper)polarizability density

From the relation between many-electron and reduced one-electron densities, the reduced one-electron nth-order (hyper)polarizability density is related to the M-electron nth-order (hyper)polarizability density as

$$\rho^{(n)}(x)=M\int \rho^{(n)}(x_1,x_2,\ldots,x_M)dx_2\cdots dx_M . \tag{24}$$

Therefore, the α and γ are also expressed by

$$\alpha=-\int\left(\sum_i^M x_i\right)\rho^{(1)}(x_1,x_2,\ldots,x_M)dx_1dx_2\cdots dx_M \tag{25}$$

and

TABLE I. Parameters used in the FF-MEWP method.

Parameter description	Value
Number of spatial grid points N	401
Size of spatial grid interval Δx	0.05 a.u.
Width Δt of time slices	$2\pi/100$ a.u.
Momentum p for initial wave packet 1	0.0 a.u.
Position of the center of initial wave packet 1	Position of nucleus **A**
Width σ of initial wave packet 1	1.0 a.u.
Momentum p for initial wave packet 2	0.0 a.u.
Position of the center of initial wave packet 2	Position of nucleus **B**
Width σ of initial wave packet 2	1.0 a.u.
Minimum electric field F	0.005 a.u.

$$\gamma=-\frac{1}{3!}\int\left(\sum_i^M x_i\right)\rho^{(3)}(x_1,x_2,\ldots,x_M)dx_1dx_2\cdots dx_M, \tag{26}$$

where the $\rho^{(1)}(x_1,x_2,\ldots,x_M)$ and $\rho^{(3)}(x_1,x_2,\ldots,x_M)$ are defined respectively by

$$\rho^{(1)}(x_1,x_2,\ldots,x_M)=\left.\frac{\partial\rho(x_1,x_2,\ldots,x_M,F)}{\partial F}\right|_{F=0} \tag{27}$$

and

$$\rho^{(3)}(x_1,x_2,\ldots,x_M)=\left.\frac{\partial^3\rho(x_1,x_2,\ldots,x_M,F)}{\partial F^3}\right|_{F=0}. \tag{28}$$

Here, the M-electron density under the static electric field F is obtained by

$$\rho(x_1,x_2,\ldots,x_M,F)=\psi^*(x_1,x_2,\ldots,x_M,F)\times\psi(x_1,x_2,\ldots,x_M,F), \tag{29}$$

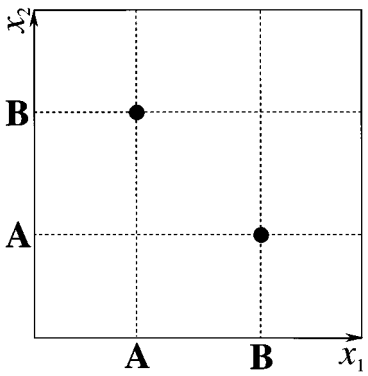

FIG. 5. Positions of the centers of the initial wave function are represented by black circles. Dotted lines indicate the positions of nuclei **A** and **B**.

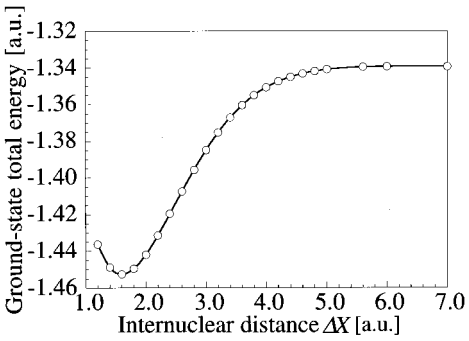

FIG. 6. Potential-energy curve for the singlet ground-state of the one-dimensional H_2 calculated by the MEWP method.

where $\psi(x_1,x_2,\ldots,x_M,F)$ denotes a spatial wave function under the static electric field F. These M-electron (hyper)polarizability densities are calculated numerically as

$$\rho^{(1)}(x_1,\ldots,x_M)=\{\rho(x_1,\ldots,x_M,F)-\rho(x_1,\ldots,x_M,-F)\}/2F \tag{30}$$

and

$$\rho^{(3)}(x_1,\ldots,x_M)=\{\rho(x_1,\ldots,x_M,2F)-\rho(x_1,\ldots,x_M,-2F)-2[\rho(x_1,\ldots,x_M,F)-\rho(x_1,\ldots,x_M,-F)]\}/2(F)^3. \tag{31}$$

We next propose a method for analysis based on the many-electron (hyper)polarizability density. The procedure for evaluating spatial contributions from their densities is basically the same as that in the reduced one-electron hyperpolarizability density analysis mentioned in the Sec. III A. The two-electron (hyper)polarizability density for the one-dimensional two-electron system is considered for simplicity and for the latter application (see Sec. IV). Similarly to the case for the reduced one-electron (hyper)polarizability density analysis, we consider two pairs of positive and negative localized densities on the two-electron coordinate plane. They are located symmetrically with respect to the diagonal line $x_1=x_2$, since the two electrons cannot be distinguished. Here, let us draw arrows from positive to negative densities, similarly to the thick arrow shown in Fig. 3. In this case, we can draw arrows from positive (white circle) to negative (black circle) densities in two ways, as shown in Fig. 4(a). In the first way, two vectors (**s** and **s**′) are symmetric with respect to a diagonal line $x_1=x_2$, while in the second one, two

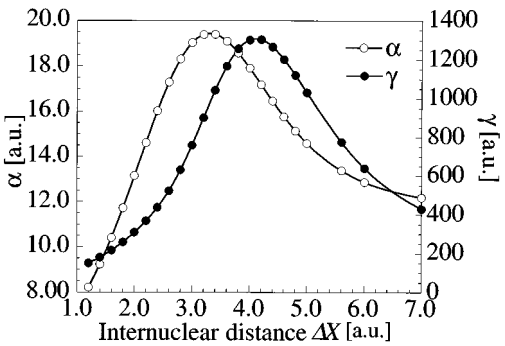

FIG. 7. Variations in the longitudinal α and γ, with internuclear distance ΔX, for the one-dimensional H_2 calculated by the FF-MEWP method.

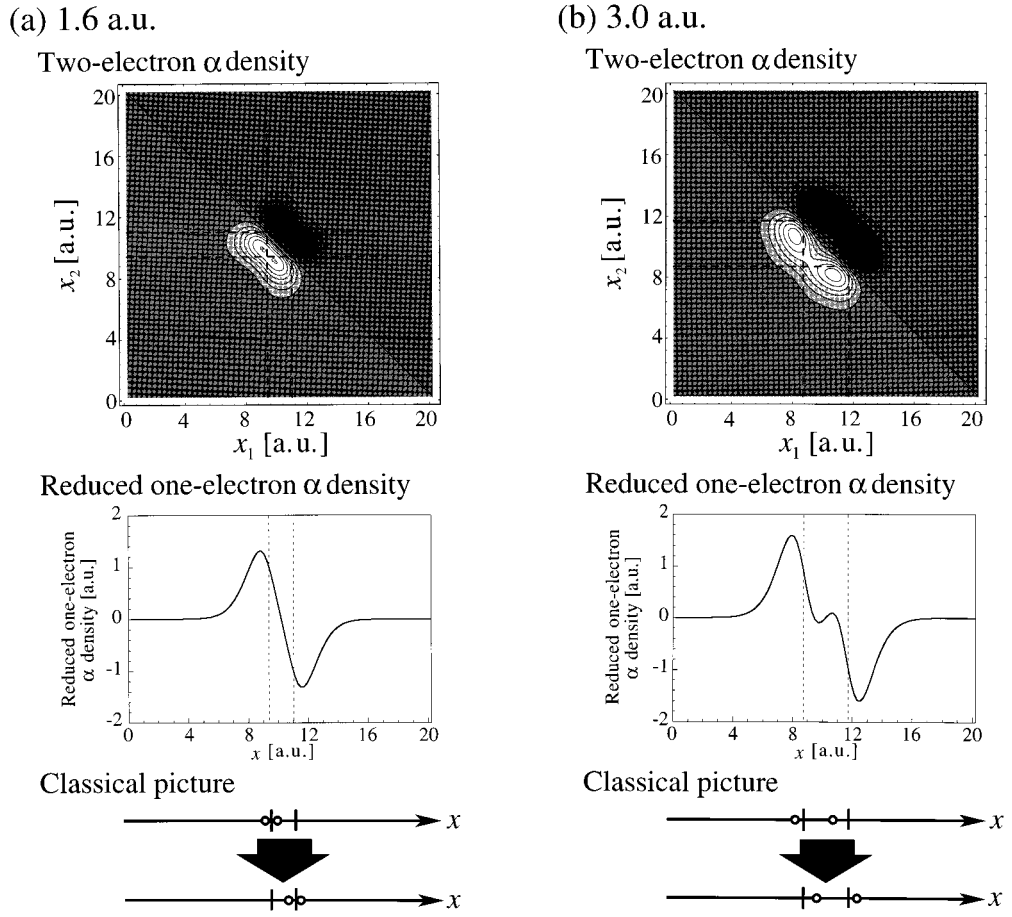

FIG. 8. Two-electron α densities, reduced one-electron α densities, and classical pictures of polarization primarily contributing to α at each internuclear distance: (a) 1.6 a.u., (b) 3.0 a.u., (c) 4.0 a.u., and (d) 6.0 a.u. In density plots, dotted lines depict the positions of the nuclei. Contour lines are drawn from -0.35 to 0.35 a.u. (contour step, 0.05 a.u.). In classical pictures, ticks and white circles indicate the positions of nuclei and electrons, respectively. Thick arrows represent the displacements of two-electron configurations.

vectors ($\mathbf{t}$ and $\mathbf{t}'$) intersect each other across the diagonal line $x_1=x_2$. Let us focus on the contribution from vector $\mathbf{s}$. We decompose the vector $\mathbf{s}$ into vector components $\mathbf{s}_1$ and $\mathbf{s}_2$, which are along the coordinates x_1 and x_2, respectively. The contribution from the vector $\mathbf{s}$ is obtained by adding the contributions from the vectors $\mathbf{s}_1$ and $\mathbf{s}_2$. The sign of the contribution becomes positive when the directions of $\mathbf{s}_1$ and $\mathbf{s}_2$ coincide with the positive direction of the coordinates x_1 and x_2, respectively. The magnitude of the contribution from the vector $\mathbf{s}_i$ ($i=1,2$) increases by increasing the distance $|\mathbf{s}_i|$ and by increasing the magnitude of the two localized densities.

In quantum theory, the position of an electron cannot be determined, and an electron wave function is extended in space. In this context, a choice of the position of an electron in the two-dimensional plane corresponds to an extraction of a classical picture of the electron. From this viewpoint, a choice of a vector drawn from the positive to the negative two-electron (hyper)polarizability density corresponds to an extraction of the classical picture of polarization relating to the (hyper)polarizability specified by the vector. In Fig. 4(b), four classical pictures of polarization corresponding to the vectors ($\mathbf{s}$, $\mathbf{s}'$, $\mathbf{t}$, and $\mathbf{t}'$) are shown as classical displacements of two-electron configurations at the starting and terminal points of these vectors. These classical displacements are divided into two types. The first type of displacement obtained by the vectors $\mathbf{s}$ and $\mathbf{s}'$ has no interchange of electrons **1** and **2** in the polarization process, while another type of displacement obtained by the vectors $\mathbf{t}$ and $\mathbf{t}'$ has an interchange. In general, therefore, multiple classical pictures can be extracted from the same pair of positive and negative (hyper)polarizability densities. In this study, however, the differences in the electrons' number are not considered, since the (hyper)polarizability relates only to the displacement of the middle point of the coordinates of the two electrons.

IV. POTENTIAL ENERGY, α AND γ, FOR ONE-DIMENSIONAL H_2 IN THE DISSOCIATION PROCESS

A. Potential-energy curve for one-dimensional H_2

One-dimensional H_2 is examined as one of the most fundamental low-dimensional systems with two electrons in quantum optics. Table I summarizes the parameters used in the FF-MEWP calculations of the species. The internuclear distance is varied from 1.2 to 7.0 a.u. Two initial wave packets are set on the positions of two nuclei, respectively. Thus the initial wave function is located as shown in Fig. 5. The singlet wave function has no nodes in the real coordinate space, as seen from Eq. (4). The potential curve for one-

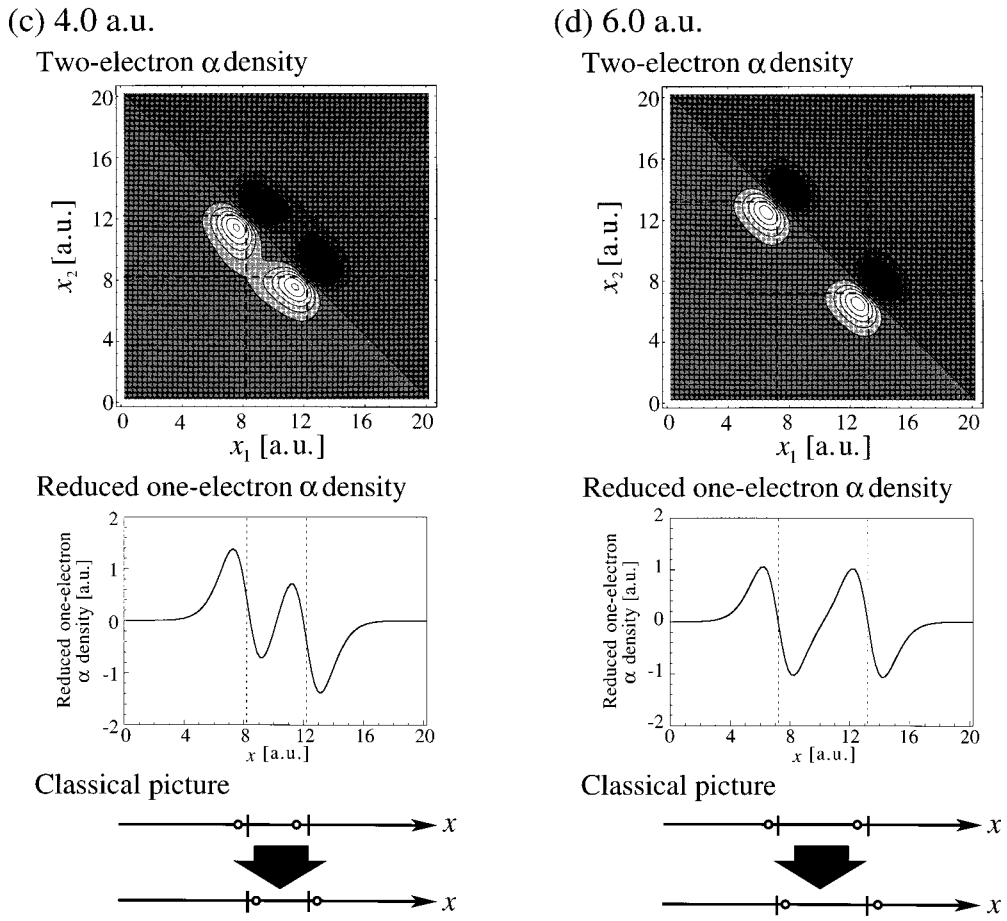

FIG. 8 (*Continued*).

dimensional H_2 is shown in Fig. 6. The equilibrium nuclear distance ($\approx$1.6 a.u., obtained by the MEWP method is found to be slightly larger than the numerically exact value ($\approx$1.4 a.u.) obtained by Kolos and Wolniewicz [12]. This feature is considered to be caused by using the softened Coulombic potential [Eq. (7)]. Details of the characteristics of the potential curve obtained by the MEWP method are discussed in connection with some approximate Coulombic potentials [5]. As a result, it is found that the qualitative shape of the potential curve obtained by the MEWP method is nearly equal to that of the numerically exact calculation, although the absolute value of the system obtained by the MEWP method is different from those of the real three-dimensional H_2.

B. Variations in α and γ in the dissociation process

Figure 7 shows the variations in the longitudinal α and γ in the dissociation process of the one-dimensional H_2. Similarly to previous *ab initio* calculation results [1,2], α has a maximum around the internuclear distance, $\Delta X = 3.4$ a.u. Although the absolute value of maximum α (15.8 a.u.) in this model obtained by the FF-MEWP method is different from the precise value (19.4 a.u.) obtained by the *ab initio* calculation for real H_2 [1], the characteristics of the variation in α are found to reproduce the *ab initio* results.

In contrast, it is found that γ has a maximum at a larger distance compared with the case of α, and γ increases more slowly at a nuclear distance of less than 3.0 a.u. For the validity of these MEWP results, we must first consider the effects of the softened Coulombic potential on the (hyper)polarizabilities. The use of this potential has two types of influence on electronic structures. One is caused by the effects on the electron-nucleus interaction, and the other is caused by the effects on the electron-electron interaction. Since electrons distributed far from nuclei are known to primarily contribute to the (hyper)polarizability, the use of the softened Coulombic potential is considered to have a primary influence on the (hyper)polarizability by reducing the Coulomb repulsion for an electron pair with short interelectronic distance nearly equal to or less than the spatial grid interval Δx. As mentioned above, however, the (hyper)polarizability is found to be essentially characterized by electron distributions from extended and diffuse spatial regions. Therefore, qualitative features of (hyper)polarizability could be meaningfully discussed if we used a sufficiently small grid Δx and a sufficiently large coordinate plane. Judging from the agreement of the shape of the potential-energy curve and the variation in α with those of real H_2, the characteristics of γ obtained here are considered to reproduce those of longitudinal γ for real H_2.

The maximum γ at $R \cong 4.0$ a.u. implies that both theoretical and experimental searches of species with chemical bonds in the intermediate correlation regime are important in relation to the molecular design of nonlinear optical materi-

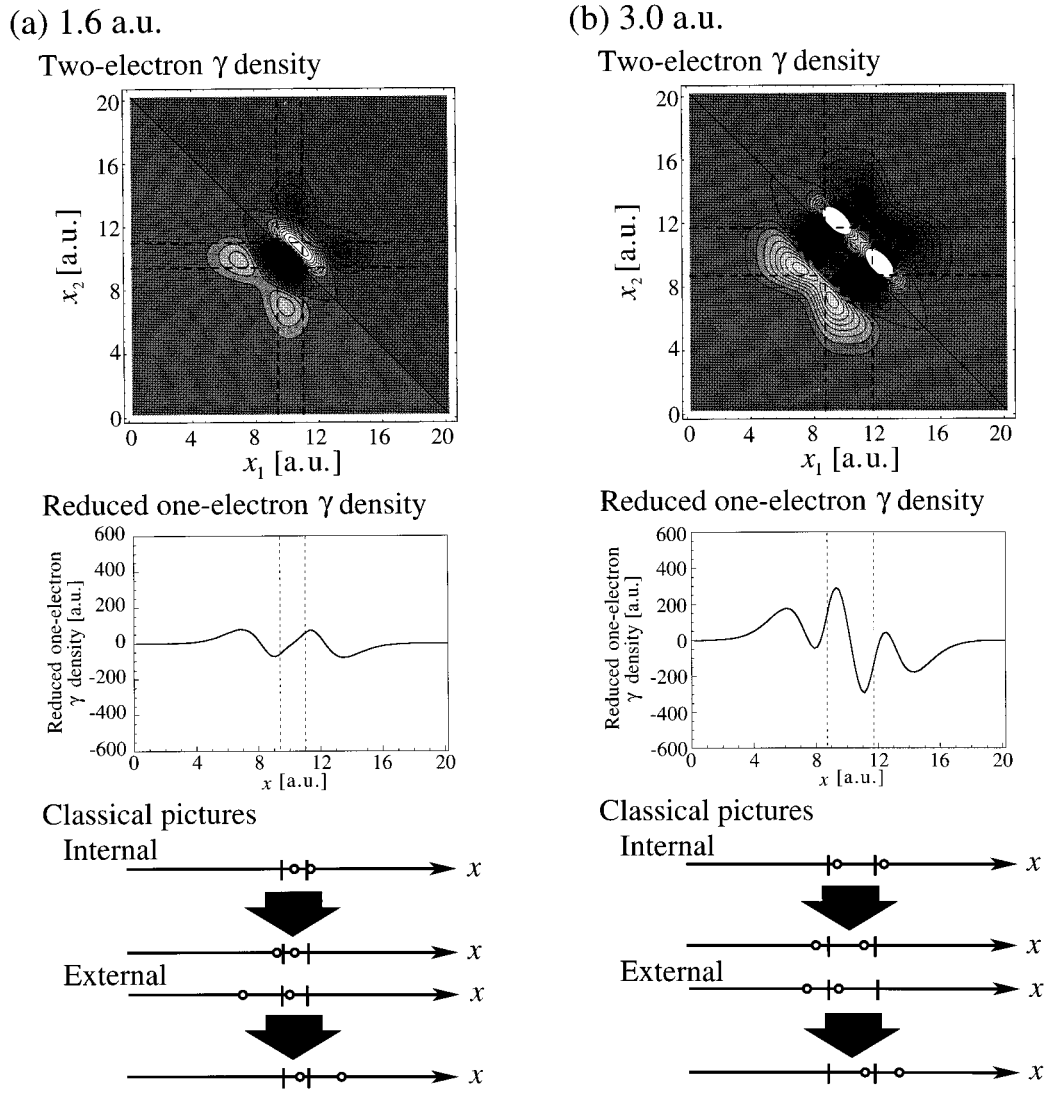

FIG. 9. Two-electron γ densities, reduced one-electron γ densities, and classical pictures of polarization primarily contributing to γ at each internuclear distance: (a) 1.6 a.u., (b) 3.0 a.u., (c) 4.0 a.u., and (d) 6.0 a.u. Contour lines are drawn from -50 to 50 a.u. (contour step, 5 a.u.). Classical pictures corresponding to internal and external two-electron γ densities are shown. See Fig. 8 for further legends.

als; e.g., π-conjugated compounds with labile chemical bonds [3,14].

C. Classical pictures based on two-electron and reduced one-electron α density analyses

The two-electron and reduced one-electron α densities at 1.6, 3.0, 4.0, and 6.0 a.u. are shown in Fig. 8. The four maximum points of positive and negative two-electron α densities are found to be located around the nuclei. Two pairs of positive and negative maximum points located symmetrically with respect to the diagonal line $x_1=x_2$ are stretched and divided along another diagonal line $x_2=-x_1+20$ with the increase in the internuclear distance. In the reduced one-electron α density plots, the region with the negative contribution to α develops at a distance larger than 3.0 a.u. This feature can be understood as the beginning of the appearance of the α density of each H atom shown in Fig. 8(d).

Here, we introduce classical pictures of electronic structures, i.e., radical and ionic structures, for the one-dimensional H_2 model. For the radical structure, two electrons (shown by the symbol ○) are located near the nuclei (shown by +), respectively. In contrast, for the ionic structure, both of electrons are located near either of the two nuclei. By using these classical pictures, the variations in polarizability during the dissociation process are found to be caused by the change from the polarization in an ionic structure to that in a radical structure. The rapid increase in α at an internuclear distance of less than 3.0 a.u. is considered to correspond to the polarization in the ionic structure. In contrast, the decrease in the polarization in the ionic structure and the increase in that in the radical structure seem to cause the decrease in α at a distance larger than 3.4 a.u.

D. Classical pictures based on two-electron and reduced one-electron γ density analyses

From the two-electron γ density plots shown in Fig. 9, we can see four pairs of positive and negative densities con-

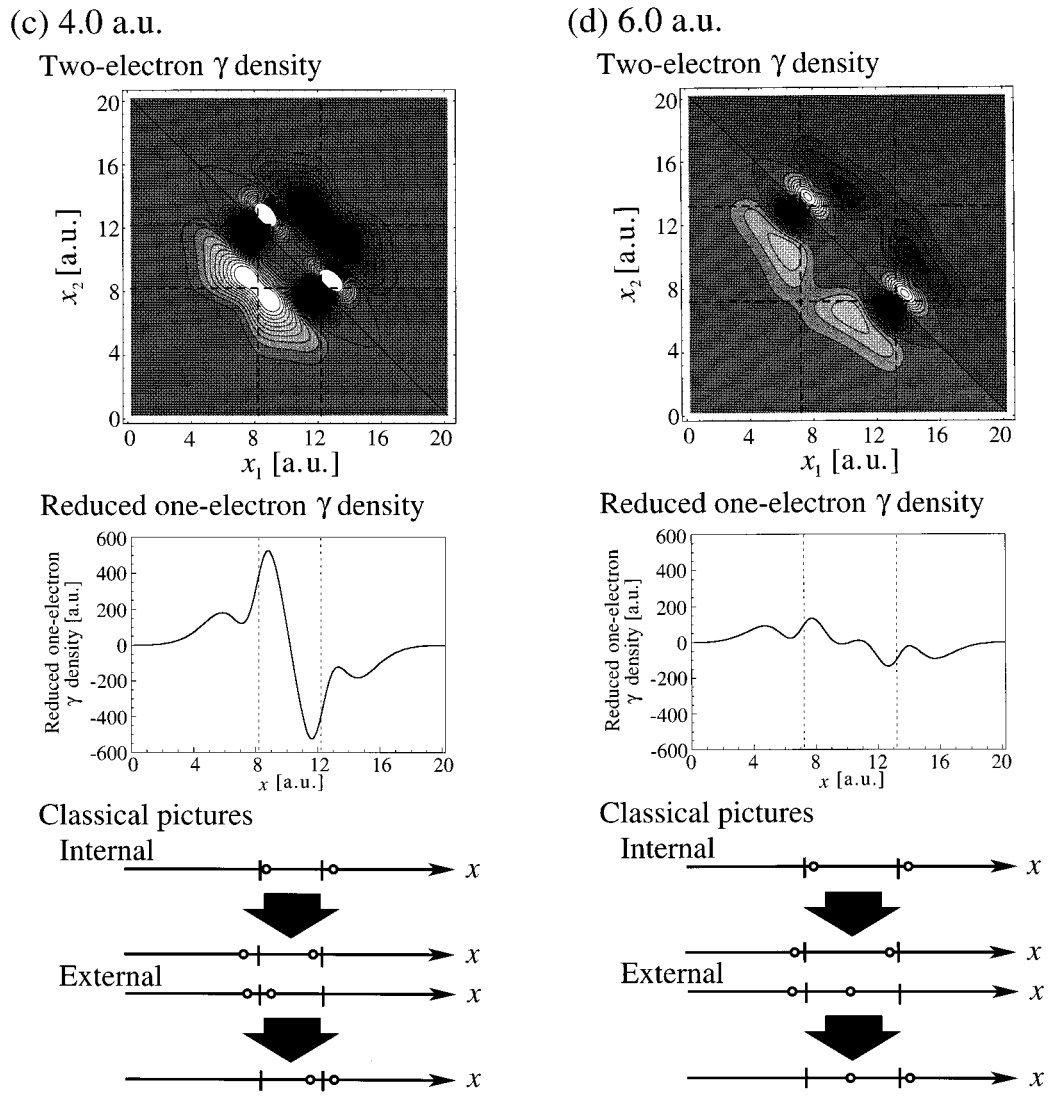

FIG. 9 (*Continued*).

structed from two internal and external pairs that give negative and positive γ's, respectively. The internal pairs represent the two pairs of densities near the line $\chi_2=-\chi_1+20$ a.u. The external pairs represent the two pairs of densities remote from the line $\chi_2=-\chi_1+20$ a.u. This feature can also be understood by the negative contribution in the bond region and the positive one in the outer region in the reduced one-electron γ density plots at the equilibrium distance (1.6 a.u.).

In general, γ is composed of contributions from three types of virtual excitation process. The perturbative formula of static γ is expressed by [13–16]

$$\gamma(0)=\sum_n \frac{(\mu_{n1})^2(\Delta\mu_{nn})^2}{E_{n1}^3}-\sum_{n,m}\frac{(\mu_{n1})^2(\mu_{m1})^2}{E_{n1}E_{m1}^2} +\left(\sum_{n\neq m}\frac{\mu_{1n}\Delta\mu_{nn}\mu_{nm}\mu_{m1}}{E_{n1}^2E_{m1}} +\sum_{n'\neq m\neq n}\frac{\mu_{1n}\mu_{nm}\mu_{mn'}\mu_{n'1}}{E_{n1}E_{m1}E_{n'1}}\right), \tag{32}$$

where μ_{ij} is a transition moment between states i and j, $\Delta\mu_{ii}$ is a difference in the dipole moments between states i and 1 (the ground state), and E_{i1} is the transition energy of state i. The numerators of each term on the right-hand side of Eq. (32) characterize the virtual excitation paths involved in each term. The three types of virtual excitation path specified by the first, second, and third terms are represented respectively by type I (1-n-n-n-1), type II (1-n-1-m-1), and type III (1-n-m-n'-1) contributions. The type-I contributions vanish for the centrosymmetric systems because of the disappearance of their dipole moments. As seen from Eq. (32), the type-I contributions are positive, while the type-II contributions are negative. Although the type-III contributions can take both positive and negative values, in principle, the type-III contributions are usually positive. The magnitudes and the signs of total γ are determined by the balance among these contributions. The three-type analysis for various compounds based on the virtual excitation processes of γ is discussed in detail elsewhere [14,17]. Therefore, the difference between internal and external contributions in the two-electron γ density is considered to be ascribed to the two types of virtual excitation processes (type II and type III) in one-dimensional H_2. In the present case, γ is composed of type-II and -III contributions. It is presumed for H_2 that the

type-II paths mainly include the ground and low-lying ionic excited states, while the type-III paths include higher-lying ionic excited states. Therefore, the internal and external contributions seem to correspond to type-II and -III processes, respectively. With the increase of the nuclear distance, the internal two-electron γ densities are stretched and divided along the diagonal line $x_2 = -x_1 + 20$, similar to the case of α, while the external maximum region is not very divided even at the internuclear distance of 4.0 a.u.

This change in the two-electron coordinate system corresponds to the fact that a classical picture of polarization in the internal region rapidly turns from the ionic to the radical structure at a small internuclear distance of less than 3.0 a.u., while that in the external region continues to hold a polarization in the ionic structure even at larger internuclear distance ($\approx$4.0 a.u.). This tendency of the external region seems to be realized by the virtual excitation paths (type III), including higher-lying excited states that are more spread out in space than lower excited states primarily contributing to the internal region.

The slow development of γ at a nuclear distance of less than 3.0 a.u. seems to be caused by a reduction of the type-III (positive contribution) paths by the type-II (negative contribution) paths, which are predicted to have a maximum at a small internuclear distance of less than 3.0 a.u., since the excited states involved mainly in the virtual excitation paths for α seem to be the same as those of type II for γ.

V. CONCLUDING REMARKS

Many-electron (hyper)polarizability density is found to offer more information that is useful in evaluating the relations between the classical displacements of electron configurations and the quantum nonlinear optical processes. For real three-dimensional systems with more electrons, however, a direct visualization of contributions from many-electron (hyper)polarizability densities in multidimensional space is hard to realize. The method for extraction of classical pictures from pairs of maximum positive and negative (hyper)polarizability densities is helpful in obtaining the characteristics of the main contributions to (hyper)polarizabilities for these systems. This method of analysis is also highly applicable to various methods treating static response properties.

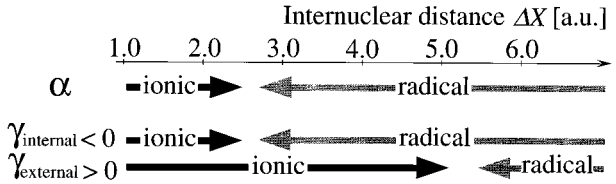

FIG. 10. Variations in classical polarization pictures mainly contributing to α and γ during the dissociation process of one-dimensional H_2. The γ_{internal} and γ_{external} represent γ's contributed from internal and external two-electron γ densities shown in Fig. 9, respectively (see Sec. IV D).

α and γ are found to increase exceptionally in the dissociation region of one-dimensional H_2. It is also found that γ reaches a maximum at a larger internuclear distance compared with the case of α. In the classical picture, this feature is considered to originate in the polarization in the ionic structure extracted from the external region in the two-electron γ density plot. Figure 10 summarizes variations in classical polarization pictures mainly contributing to α and γ during the dissociation process of the one-dimensional H_2.

The present study suggests that the variations in (hyper)polarizability in the dissociation and unstable regions for systems with more electrons will present many unexpected and exciting phenomena for experimental and theoretical investigation. In fact, nonlinear optical responses of systems in the strong and intermediate correlation regimes are currently attracting attention in relation to many applications. The pictorial and intuitive method of analysis developed here will be useful for the study of such phenomena. Further, the success of the present analysis based on the FF-MEWP method indicates its fruitful application to theoretical investigations of dynamic responses to time-dependent external fields by using the concept of dynamic hyperpolarizability density [17]. Such applications are currently being studied.

ACKNOWLEDGMENT

We are grateful to the Ministry of Education, Science and Culture of Japan (Specially Promoted Research No. 06101004) for financial support.

[1] P. A. Hyams, J. Gerratt, D. L. Cooper, and M. Raimondi, J. Chem. Phys. **100**, 4417 (1994).
[2] B. Champagne, V. Deguelle, and J. M. André, J. Mol. Struct. (Theochem.) **332**, 93 (1995).
[3] M. Nakano, I. Shigemoto, S. Yamada, and K. Yamaguchi, J. Chem. Phys. **103**, 4175 (1995).
[4] S. Yamada, M. Nakano, I. Shigemoto, and K. Yamaguchi, Chem. Phys. Lett. **254**, 158 (1996).
[5] H. Nagao, M. Nakano, S. Yamanaka, Y. Shigeta, S. Yamada, D. Yamaki, I. Shigemoto, S. Kiribayashi, and K. Yamaguchi, Int. J. Quantum Chem. Symp. (to be published).
[6] J. Javanainen, J. H. Eberly, and Q. Su, Phys. Rev. A **38**, 3430 (1988); Q. Su and J. H. Eberly, *ibid.* **44**, 5997 (1991).
[7] K. Kasuga, S. Tanaka, and S. Yamashita (unpublished).
[8] R. Kosloff and H. Tal-Ezer, Chem. Phys. Lett. **127**, 223 (1986).
[9] P. Chopra, L. Carlacci, H. F. King, and P. N. Prasad, J. Phys. Chem. **93**, 7120 (1989).
[10] M. Nakano, K. Yamaguchi, and T. Fueno, Chem. Phys. Lett. **185**, 550 (1991).
[11] M. Nakano, K. Yamaguchi, and T. Fueno, Nonlinear Opt. **6**, 289 (1994).
[12] W. Kolos and L. Wolniewicz, J. Chem. Phys. **49**, 404 (1968).
[13] M. Nakano, M. Okumura, K. Yamaguchi, and T. Fueno, Mol.

Cryst. Liq. Cryst. **182A**, 1 (1990).
[14] M. Nakano and K. Yamaguchi, Chem. Phys. Lett. **206**, 285 (1993).
[15] M. Nakano and K. Yamaguchi, Phys. Rev. A **50**, 2989 (1994).
[16] M. Nakano, K. Yamaguchi, Y. Matsuzaki, K. Tanaka, and T. Yamabe, J. Chem. Phys. **102**, 2986 (1995); **102**, 2996 (1995); Chem. Phys. Lett. **233**, 411 (1995).
[17] M. Nakano, S. Yamada, I. Shigemoto, and K. Yamaguchi, Chem. Phys. Lett. **250**, 247 (1996).